

****FULL TITLE****

*ASP Conference Series, Vol. **VOLUME**, **YEAR OF PUBLICATION***

****NAMES OF EDITORS****

Dust in the Early ($z>1$) Universe

Fabian Walter

Max Planck Institut für Astronomie Heidelberg, Germany

Abstract. Although dust emission at cosmological distances has only been detected a little more than a decade ago, remarkable progress has been achieved since then in characterizing the far-infrared emission of high-redshift systems. The mere fact that dust can be detected in galaxies at high redshift is remarkable for two reasons: (a) even at very early cosmic epochs (all the way to the first Gyr of the universe), dust production was apparently very effective, (b) due to the inverse K-correction ('the magic of (sub-)millimeter') is it actually possible to detect this dust emission using current facilities. Deep blind surveys using bolometer cameras on single dish telescopes have uncovered a population of massively starforming systems at $z\sim 2$, the so-called submillimeter galaxies (SMGs). Follow-up radio and millimeter interferometric observations helped to characterize their main physical properties (such as far-infrared luminosities and implied star formation rates). Average FIR properties of fainter optically/NIR-selected classes of galaxies have been constrained using stacking techniques. Targeted observations of the rare quasars have provided evidence for major star formation activity in quasar host galaxies throughout cosmic times. Molecular gas and PAH features have been detected in both SMGs and quasars, providing additional evidence for major star formation episodes ($\text{SFR}\sim 500\text{--}3000\text{ M}_{\odot}\text{ yr}^{-1}$) in the brightest systems. Even though remarkable progress has been achieved in recent years, current facilities fail to uncover the counterparts of even major local starbursts (such as Arp 220) at any significant redshift ($z>0.5$). Only ALMA will be able to go beyond the tip of the iceberg to study the dust and FIR properties of typical star forming systems, all the way out to the epoch of cosmic reionization ($z\gg 6$).

1. Some Thoughts/Disclaimer

This conference (Cosmic Dust – Near and Far) covered an impressive range of topics related to dust in the universe. Dust emission from evolved stars and supernovae, protoplanetary and debris disks, as well as our solar system was discussed in detail. One session was dedicated to the global dust emission in our Galaxy as well as in other galaxies — and a particular emphasis was put on recent laboratory studies of dust and the modeling of dust emission and evolution. Progress in this field of research has clearly been dramatic in the last decade!

I was asked to review the subject of 'Dust at high redshifts', a subject that has exploded in recent years: only a decade ago, hardly any observations of high-redshift dust existed. In the following I will attempt to summarize key aspects of dust at high redshift and discuss some of the recent results — this review cannot be complete and the reader may forgive me for not giving credit to everybody's work that has been published on this subject. In this review, I will

try to address a mainly ‘Galactic’ audience/reader as most of the presentations at the conference were centred around Galactic dust emission. For further reading, the interested reader is also referred to some excellent reviews in the literature (e.g., Blain et al. 2002, Ivison 2001, Smail et al. 2002, 2003, Solomon & Vanden Bout 2005, Smail 2006).

2. The Magic of (Sub-)millimeter

Even with current (sub-)millimeter cameras it is not trivial to map the dust emission in nearby galaxies (e.g. Guélin et al. 1995, Thomas et al. 2002, Meijering et al. 2005, Bendo et al. 2006, Weiss et al. 2008). How is it then possible that dust can be detected out to the highest redshifts with the same instruments? Together with the fact that some systems at high redshifts are very luminous, the main reason for this astonishing fact is what people refer to as the ‘magic of (sub-)millimeter’. This is illustrated in Figure 1: Here the spectral energy distribution (SED) of the ultraluminous infrared galaxy (ULIRG) Arp 220 (a template commonly used in extragalactic astronomy) is plotted as a function of different redshifts (from $z=0.1$ to 10). Two things are immediately clear from this plot: (1) The emission gets fainter and (2) the emission is being redshifted as a function of redshift. However, if one were to observe such an object at ~ 1 mm wavelengths (indicated by the vertical dashed line for a hypothetical observation with MAMBO), the observed flux density stays roughly constant for any redshift in the range $0.5 < z < 10$! This is due to the fact that the peak

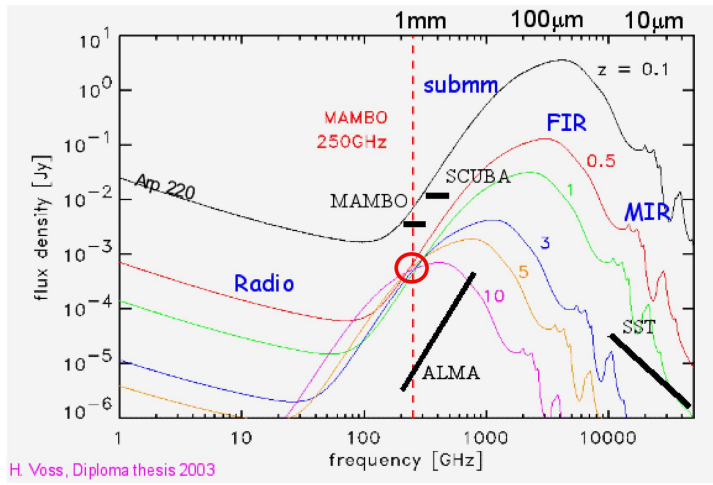


Figure 1. The observed spectral energy distribution of Arp 220 as a function of redshift. The horizontal dashed line indicates the observing wavelength at ~ 1 mm (e.g., using the MAMBO bolometer). The observed flux density at this frequency is almost independent of redshift for $0.5 < z < 10$ (as indicated by the circle). This is the reason why high-redshift dust emission can be detected given current instrumentation (‘magic of (sub-)millimeter’). Short horizontal bars indicate ~ 4 sigma sensitivities for MAMBO and SCUBA, respectively. Figure adopted from Voss (2003).

of the SED is shifted towards the observed frequency – in other words, the shift towards the peak of the SED cancels out the dimming due to the increased redshift (‘inverse K correction’). This immediately implies that the flux density observed of a source at $z \geq 1$ in the millimeter regime is not a function of redshift/distance, it only is a function of the intrinsic luminosity of the source. This situation is obviously in stark contrast to what would be seen at any other wavelength (X-ray/UV/optical/IR/radio), and is, at first glance, contrary to sanity and reason. It should be noted though that in the example discussed here (Arp 220) the sensitivities of current bolometers (e.g. MAMBO) are an order of magnitude too high to detect an Arp 220 counterpart (with an intrinsic FIR luminosity of $5 \times 10^{12} L_{\odot}$) at significant redshifts (see short horizontal bar in Figure 1). In other words, current instruments only allow one to observe the brightest objects at any redshift (as discussed further below). But it is immediately clear that ALMA will have no problem detecting objects that are more than an order of magnitude fainter than Arp 220 (as indicated by the diagonal line in Figure 1).

This effect is discussed in more detail in Blain et al. (2002): Figure 2 shows the result of his models: the flux density of a source with $L_{\text{FIR}} = 5 \times 10^{12} L_{\odot}$ is plotted as a function of redshift for various observing bands. It is clear that both the optical and radio flux densities drop dramatically as a function of redshift, whereas the flux densities stay roughly constant for observations at ~ 1 mm.

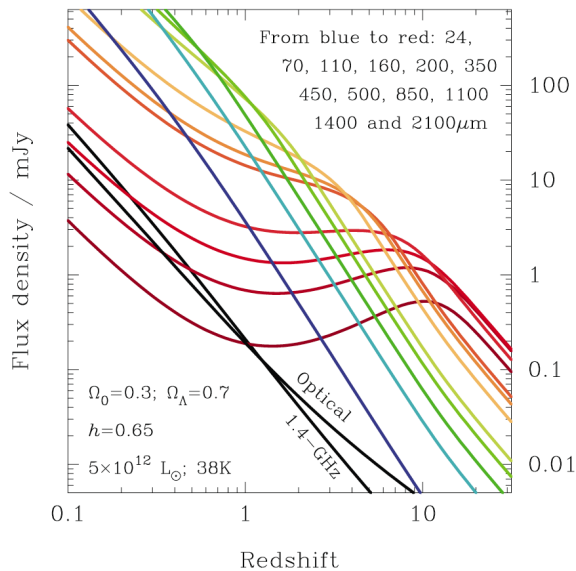


Figure 2. A more detailed description of the situation described in Figure 1: Here the measured flux density of a source of $L_{\text{FIR}} = 5 \times 10^{12} L_{\odot}$ is plotted as a function of redshift for various observing bands. At around 1 mm wavelengths the measured flux density stays approximately constant as a function of redshift. For comparison, the flux densities in the optical and radio are also shown. Figure taken from Blain et al. (2002).



Figure 3. Graphical illustration for the fact that the measured flux densities at (sub-)millimeter wavelengths at high redshifts are roughly constant as a function of redshifts. Top: Simulation of an ALMA deep field, where the left panels shows galaxies at $z < 1.5$ and the right panel shows galaxies at $z > 1.5$. This relation of number densities of detected galaxies is opposite to what is seen in the optical (bottom panels). Top images from Wootten & Gallimore (2000). Bottom images from K. Lanzetta, K. Moore, A. Fernandez-Soto, and A. Yahil (SUNY) (courtesy of Kenneth M. Lanzetta).

It is this ‘inverse K correction’ that allows us to observe objects at significant redshifts at all!

This ‘magic of submillimeter’ can be illustrated further by simulated ALMA deep field observations as shown in Figure 3: In the top panel, galaxies in an ALMA deep field are separated into low-redshift ($z < 1.5$) and high-redshift ($z > 1.5$) objects (left and right panels, respectively). Due to the reason discussed above, there will be many more objects that are detectable at high redshifts. This situation is opposite to what is seen in the optical (bottom two panels, see figure caption for full credits).

There are basically two observing strategies for studying the dust properties of high redshift systems: (A) blind searches using blank field observations and (B) targeted observations of rare objects. Both strategies are discussed in the following.

3. Blank (deep) fields

The revolution of high-redshift studies of dusty galaxies started in the late 1990’s with the discovery of (sub-)millimeter bright galaxies (‘SMGs’) using the

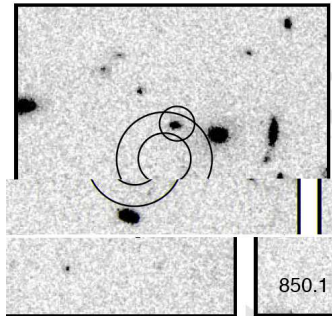


Figure 4. The case of HDF850.1, the brightest sub-millimeter source discovered by SCUBA in the Hubble deep field. The circle indicates the position of the SCUBA source whereas the grey scale represents the deep HST imaging. No obvious counterpart can be identified from these observations (see text for further details). Figure taken from Hughes et al. (1998).

SCUBA (JCMT) and MAMBO (IRAM 30m) bolometers (Smail et al. 1997, Bertoldi et al. 2000, Smail et al. 2002, Ivison et al. 2002, Cowie et al. 2002, Dannerbauer et al. 2002, and many more!). One of the most famous studies is the SCUBA deep field study of the Hubble Deep Field (HDF) by Hughes et al. (1998) which showed that the brightest submillimeter emission in the field did not show an obvious counterpart in deep HST imaging, as shown in Figure 4 (subsequent studies aimed at identifying a counterpart, Downes et al. 1999, Dunlop et al. 2004). This difficulty of identifying the correct optical/NIR counterpart (which can be straightforwardly explained by the ‘negative K correction’ discussed above if the source is at high redshift) has been plaguing many of the subsequent (sub-)millimeter deep field studies: without a secure identification at optical/NIR wavelengths (or, in fact, at any wavelength), spectroscopic follow-up using 8–10 m glass is virtually impossible. This issue is further complicated by the fact that the beam sizes of past and current bolometers mounted on single dish telescopes are large (SCUBA: $\sim 15''$, MAMBO: $\sim 11''$), i.e., even in case there are optical/NIR sources in the immediate neighborhood of a (sub-)millimeter source, it is often difficult to tell which of the possible counterparts is in fact the correct one.

Two methods have been pushed forward to address this positional uncertainty: (A) increase of resolution in the (sub-)millimeter band using (sub-)millimeter interferometry and (B) increase of resolution by employing deep radio continuum maps (typically at 20 cm wavelengths) – both methods will be briefly discussed in the following:

Millimeter Interferometry: The most straightforward method to get better positions of the (sub-)millimeter sources of interest is by re-observing the candidates with (sub-)millimeter interferometers. This method works well in practice (e.g., Dannerbauer et al. 2002, Younger et al. 2007, Dannerbauer et al. 2008), yielding positional accuracies of $\leq 1''$. The major drawback is that these observations are expensive in terms of telescope time: typically one full track (i.e., ~ 8 hours of observing time) is needed to achieve the required sensitivity at a

(sub-)millimeter interferometer. Also, the primary beam of interferometers at ~ 1 mm wavelengths is small (e.g. in the case of the Plateau de Bure interferometer: $\sim 20''$) which implies that only one source can be followed up at a time. As an example the identification of AzTEC sources in the COSMOS deep field (Scoville et al. 2006, Scott et al. 2008) using SMA interferometry is shown in Figure 5 (Younger et al. 2007) and the identification of one of the brightest SMGs in the GOODS-North field is presented in Figure 6 (Dannerbauer et al. 2008).

Radio Interferometry: Ivison et al. (1998, 2000, 2002) and Smail et al. (2000) pioneered a different technique: identification of SMGs through their radio continuum emission. The strength of this approach lies in the fact that deep (~ 10 – $20 \mu\text{Jy}$) wide-field ($30'$) VLA radio continuum maps exist for most of the deep fields that have been looked at with (sub-)millimeter bolometers. The advantage of this technique is that the synthesized radio beam ($\sim 1''$) is much smaller than that of single dish bolometers, which in turn enables direct identification with optical/NIR sources (needed first for photometric redshift determination and subsequently for spectroscopic follow-up). The downside of this approach is obviously that sources without a radio identification can not be identified (the radio completeness in Ivison et al. is $\sim 65\%$). As the radio flux is a strong

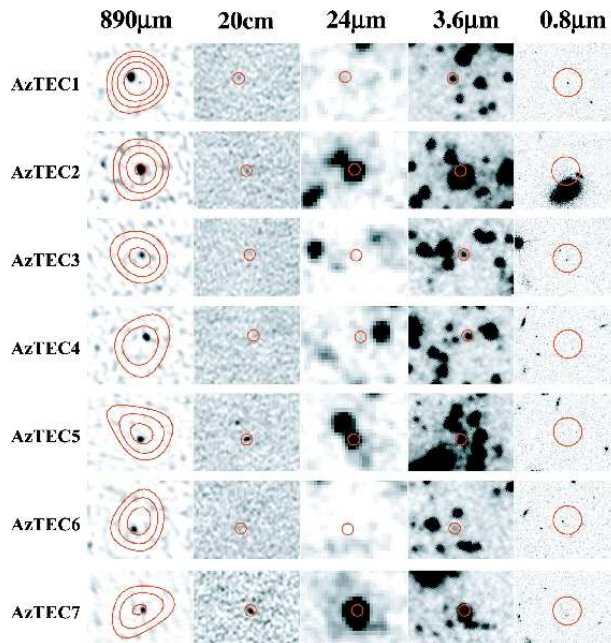


Figure 5. Example of how interferometric (sub-)millimeter observations can help to pinpoint the emission seen in deep bolometer maps (needed to identify the optical/NIR counterpart and for subsequent spectroscopic follow-up). The left panels show the AzTEC beam in contours overlaid on the SMA detections at $890 \mu\text{m}$ in the COSMOS field. Figure taken from Younger et al. (2007).

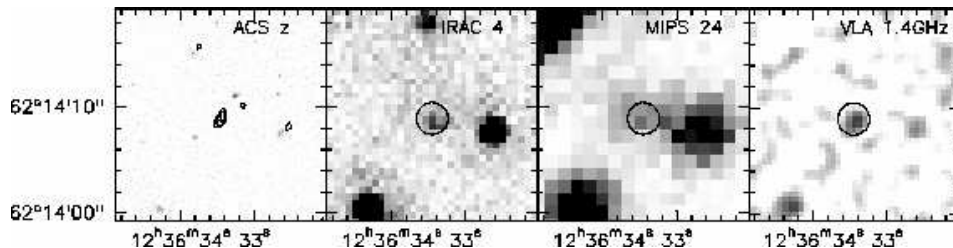


Figure 6. Example of how millimeter interferometry was used to pinpoint the location of GN10, one of the brightest sources in the GOODS-N region. Contours in the left panel indicate the position of the source as detected with the IRAM Plateau de Bure interferometer (shown as a circle in the subsequent panels). The source is now clearly identified, which enables a photometric determination of its redshift. Figure taken from Dannerbauer et al. (2008).

function of redshift (see Figure 2 above) it is likely that the radio-undetected sources are at high ($z > 4$) redshifts (see discussion below). From the samples of radio-identified SMGs, Chapman et al. (2003, 2005, Figure 7) derived a number of key properties for this population of sources: the median redshift is $z=2.3$ ($\sigma=1.3$ – similar to the median QSO redshift), and the typical FIR luminosity is $L_{\text{FIR}}=5 \times 10^{12} L_{\odot}$. Importantly, they conclude that there is a >500 decrease in ULIRG space density from redshifts $z \sim 2$ to 0, implying very strong evolution of this class of galaxies.

By now, 100s of SMGs have been detected in a number of extensive observing campaigns using SCUBA (e.g. through the SCUBA Half-Degree Extragalactic Survey SHADES, Mortier et al. 2005, Coppin et al. 2006, Ivison et al. 2007), MAMBO (e.g. Bertoldi et al. 2000, 2007), and AzTEC (e.g., Scott et al. 2008, Perera et al. 2008). Some of these surveys were targeting clusters to probe lensed background sources with the goal to extend the luminosity function of SMGs to fainter flux levels. The reader is referred to, e.g., Knudsen et al. (2006, 2008) and Coppin et al. (2007), for a discussion on the faint end of the SMG luminosity function.

3.1. Molecular gas and PAH emission in SMGs

Both molecular gas and poly-cyclic aromatic hydrocarbons (PAH) emission (both extensively discussed at this conference) have now been detected in SMGs. The molecular gas content of SMGs has been studied in a major observational campaign using the Plateau de Bure interferometer by Genzel et al. (2003), Neri et al. (2003), Greve et al. (2005), and Tacconi et al. (2006, 2008). Figure 8 shows a composite of CO spectra for SMGs (Tacconi et al. 2006) – some key results of this survey are that the implied molecular gas masses are of order $3 \times 10^{10} M_{\odot}$ (an order of magnitude more massive than the Milky Way, but comparable in mass to the QSO population at similar redshift). The CO spectra have line widths of $\sim 500 \pm 200 \text{ km s}^{-1}$, and, together with size measurements, give dynamical masses of $M_{\text{dyn}} \sim 10^{11} M_{\odot}$, implying high gas mass fraction of $\sim 20 - 50\%$ (Tacconi et al. 2008). In summary, the detection of abundant molecular gas in these system is consistent with the picture that they are major starforming systems

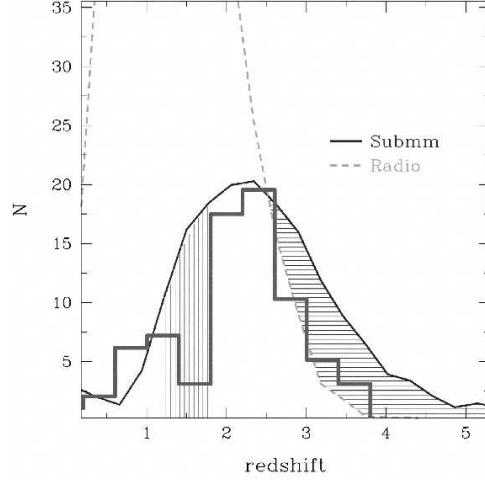


Figure 7. Histogram of the redshift distribution of radio-selected SMGs. The median redshift of this population is $z \sim 2.3$. One of the open questions is whether the decrease in SMGs at $z > 4$ is an intrinsic property of this population, or whether it is due to the fact that they are faint in the radio (and thus would not end up in the selection shown here). Figure taken from Chapman et al. (2005).

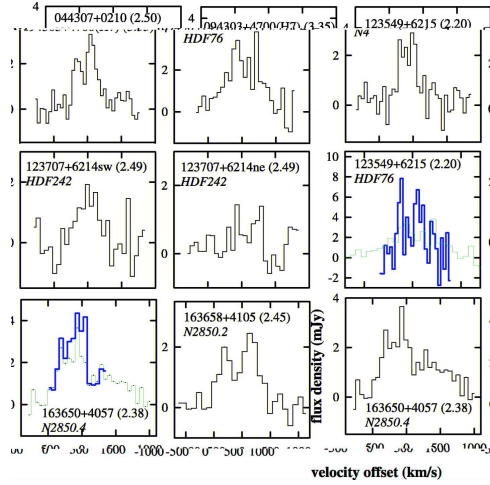


Figure 8. Integrated CO spectra of SMGs obtained with the Plateau de Bure interferometer. Typically, the CO(3–2) spectrum is shown here; the thick lines indicate higher-J CO transitions of two sources. Figure taken from Tacconi et al. (2006).

that have high FIR luminosities (as evidenced by their strong sub-millimeter emission).

Emission from PAHs has also been detected in SMGs: Figure 9 shows an average SMG spectrum at $z \sim 2.5$ obtained with the IRS on-board Spitzer (Valiante et al. 2007, see also Lutz et al. 2005, Menendez-Delmestre et al. 2007, Pope et al. 2008). Both the $6.2\mu\text{m}$ and $7.7\mu\text{m}$ PAH features are detected at high signal-to-noise and the spectrum is well fit by the nearby starburst M82 plus continuum emission. The same study noted that the PAH/continuum ratio in $z \sim 2.5$ SMGs is very similar to what is found in local ULIRGs. It has also been suggested that the PAH emission features in SMGs can be used as a proxy for the star formation rate in SMGs (e.g., Pope et al. 2008).

3.2. An SMG population at $z > 4$?

One of the open questions is how significant the SMG source population at $z > 4$ really is. Given their high redshifts, it is difficult to first identify and then spectroscopically confirm these objects. This has been pointed out early on by, e.g., Dunlop et al. (2001), Eales et al. (2003) and Ivison et al. (2005). To date only few SMGs with confirmed redshifts $z > 4$ are known: GN20, GN20.2a and GN 10 (in the GOODS North field, Daddi et al. 2009a, 2009b, Dannerbauer et al. 2008), and one source in the COSMOS field (Capak et al. 2008, Schinnerer et al. 2008). Recently, Coppin et al. (2009) identified a $z = 4.76$ submillimeter-selected source in the Extended Chandra Deep Field South using the APEX LABOCA survey (Weiss et al., in prep., see next sub-section), making this the currently highest-redshift source known that has been detected in a blind survey (Figure 10). All sources known so far at $z > 4$ are potentially very much dust enshrouded, and it is very likely that ongoing observing campaigns will soon uncover more systems

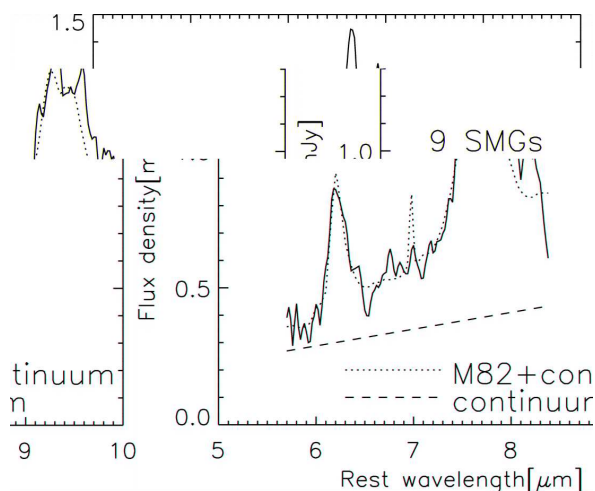


Figure 9. Composite Spitzer IRS spectrum for 9 SMGs at a median redshift of $z \sim 2.5$. The PAH features at $6.2\mu\text{m}$ and $7.7\mu\text{m}$ are clearly detected and the emission is well fit by an M82 template and an additional continuum component. Figure taken from Valiante et al. (2007).

at similar or even higher redshifts. A novel technique to select these targets is discussed in Greve et al. (2008): at very high redshift ($z > 4$), one would expect sources to be detected by MAMBO but not with SCUBA (given the respective sensitivities and the slope of the dusty SED, see again Figure 1). Greve et al. identified a number of such ‘SCUBA drop-out’ sources and argue for either a very high redshift origin of these sources, or a very cold/different dust composition than typically seen. One should keep in mind though that the total number of objects that have been detected in dust emission at $z > 4$ is much higher, i.e. targeted observations of high-redshift QSOs have resulted in a (sub-)millimeter detection rate of $\sim 1/3$ (as discussed in Section 4).

3.3. First results from LESS

The new $870\mu\text{m}$ LABOCA submillimeter camera on APEX was recently used for the LESS project (LESS: ‘The LABOCA ECDFS Submm Survey’). This survey covers the area of $\sim 0.5^\circ \times 0.5^\circ$ of the Extended Chandra Deep Field South (ECDFS), and reaches a uniform rms of 1.3 mJy over the full area. This is the largest contingent survey ever performed in the sub-millimeter and the rich auxiliary database of the ECDFS enables immediate identification of the objects in the field. Of order 100 objects are individually detected in LESS (Weiss et al., in prep.), many of which have been identified at other wavelengths (Coppin et al., in prep.). The auxiliary database also enables statistical studies of optically/NIR selected galaxies using stacking techniques. Preliminary results are shown in Figure 11, where optically/NIR selected galaxies show strong stacked submillimeter emission (Greve et al. 2009). Stacked $870\mu\text{m}$ signals are: 0.23 ± 0.02 mJy (11.5σ), 0.54 ± 0.06 mJy (10.8σ), 0.40 ± 0.04 mJy (10.0σ), and 0.46 ± 0.06 mJy (7.7σ) for the $K_{\text{vega}} < 20$, BzK [B-z,z-K-selection], ERO [extremely red objects] and DRG [distant red galaxies] samples, respectively (see Greve et al. (2009) for details on the high-redshift source selection). Splitting the

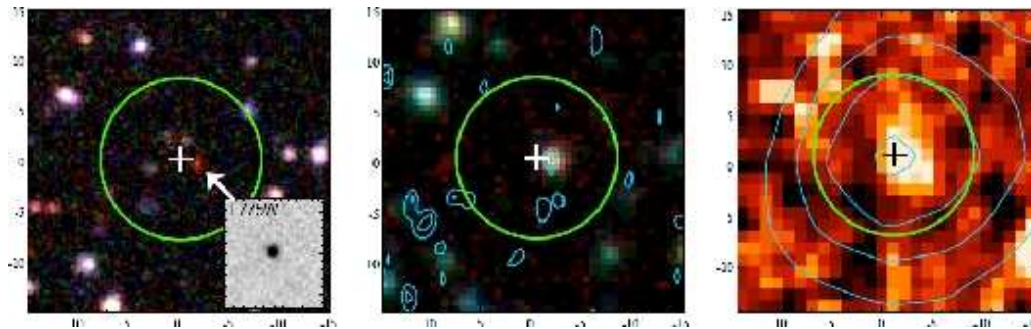


Figure 10. Identification of the highest-redshift submillimeter-selected source in the Extended Chandra Deep Field South using the LABOCA bolometer mounted on APEX. The left panel shows a VBR image from the MUSYC survey (Gawiser et al. 2006), the centre is a Spitzer IRAC composite and the right image is a $24\mu\text{m}$ image from the Spitzer-Fidel survey (Dickinson et al., in prep.). The green circle indicates the LABOCA beam, the contours in the middle panel the radio continuum emission. All scales are in arcseconds. Figure taken from Coppin et al. (2009).

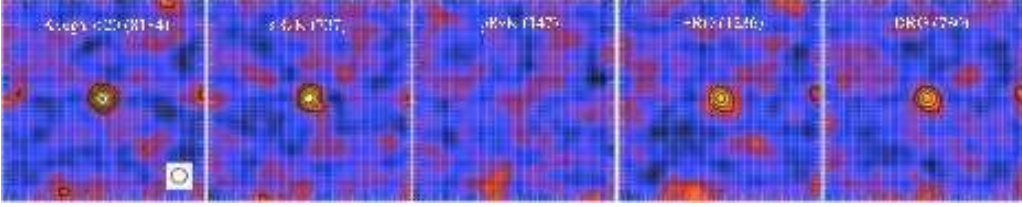


Figure 11. First $870\mu\text{m}$ stacking results of the LABOCA ECDFS Submm Survey (‘LESS’) of optically/IR selected galaxies. See text for the description and flux densities of the respective galaxy class. Figure taken from Greve et al. (2009).

BzK-selected galaxies up into star-forming (sBzK) and passive (pBzK) galaxies, the former population is significantly detected while the latter is not.

4. Targeted Observations of ‘rare objects’

The remainder of this review will focus on targeted (sub-)millimeter observations, in particular quasars. These are so rare on the sky that chances of detecting them in blind surveys are relatively slim (but see Coppin et al. 2009).

4.1. General FIR properties of high- z quasars

Dust has now been detected in many quasars at different redshifts. This is summarized in Figure 12, where L_{FIR} of the quasars is plotted as a function of redshift (Beelen et al. 2006, Omont et al. 2003, Wang et al. 2007, 2008). Here, full symbols represent detections, open symbols upper limits, dashed lines indicate the typical 3 sigma detection limits of MAMBO and SCUBA, respectively. Quite remarkably, about 1/3 of all sources are detected in the (sub-)millimeter, independent of redshift. Also, there are hardly any ‘outliers’ in this plot, indicating that the bright quasars share similar FIR properties, independent of cosmic age. A major caveat in this interpretation is the fact that currently only the tip of the iceberg can be detected with current bolometers – a situation that is unlikely to change until the advent of ALMA.

These individual dust detections can be used to construct a composite SED of all quasars (each quasar is at a different redshift, thus each measurement samples a different part of the average [restframe] SED). The result is shown in Figure 13 (Beelen et al. 2006), where the different measurements have been normalized to the FIR luminosity of one particular object (see Beelen et al. for details). It is striking how similar the dust SED looks for objects at different redshifts – amongst other things, this hints at very rapid dust enrichment in the host galaxies of these objects. In the near future, a guaranteed time Herschel key project (PI: Klaus Meisenheimer, MPIA) will sample the dusty SEDs of individual $z > 5$ quasars to unprecedented accuracy.

Another interesting finding is the location of the high-redshift quasars on the radio-FIR relation (Condon et al. 2002, Yun et al. 2001). This is shown in Figure 14, where the rest-frame 1.4 GHz luminosity is plotted as a function of

L_{FIR} for different classes of objects. The crosses show the IRAS 2 Jy sample of Yun et al. (2001); the circles indicate the quasars of Beelen (2003). The dashed line shows the mean value of q (quantifying the FIR/radio relationship, Condon 1992), while the dotted lines display the IR and radio excesses (5 times above and below the value expected from the linear far-IR/radio relation seen at low redshift). The same result holds if one adds the $z \sim 6$ quasar population (Wang et al. 2007). As noted in Beelen et al. (2003), the fact that the high- z quasars roughly follow the Condon relation for star-forming galaxies suggests that their radio and far-IR emission also arise from star formation. Some contribution to L_{FIR} by a central AGN can not be excluded, but it is unlikely that L_{FIR} is predominantly powered by a central engine.

In this context, it is also interesting to investigate the ‘star formation law’ in the highest redshifts systems (both quasars and submillimeter galaxies). In Figure 15, L_{FIR} is plotted as a function of CO luminosity (a measure for the molecular gas mass). This plot includes the sample of low- z spiral and starburst galaxies from Gao & Solomon (2004), ULIRGs from Solomon et al. (1997), $z < 0.2$ PG QSOs from Alloin et al. (1992), Evans et al. (2001), and Scoville et al. (2003), extrapolated Galactic molecular clouds (GMCs) from Mooney & Solomon (1988), the Milky Way (Fixsen et al. 1999), and high- z submillimeter galaxies, radio galaxies, and QSOs from the review by Solomon & Vanden Bout (2005). The dashed line is a fit to all sources and yields a slope of 1.4 (e.g., Riechers et al. 2007). The location of the high-redshift sources (both SMGs and quasars) suggests that the trend seen at lower redshift (‘more SF per unit CO’) continues out to the highest redshifts/luminosities. The particularly interesting finding is that the quasars and the submillimeter galaxies occupy the same parameter space (upper right corner in Figure 15). This is another indication for

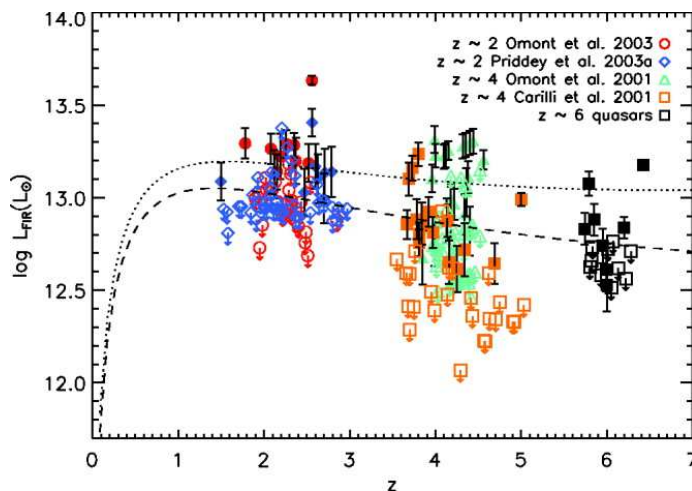


Figure 12. L_{FIR} as a function of redshift for all quasars detected so far. Full symbols represent detections, open symbols upper limits, dashed lines indicate the typical 3 sigma detection limits of MAMBO and SCUBA, respectively. Figure taken from Wang et al. (2007).

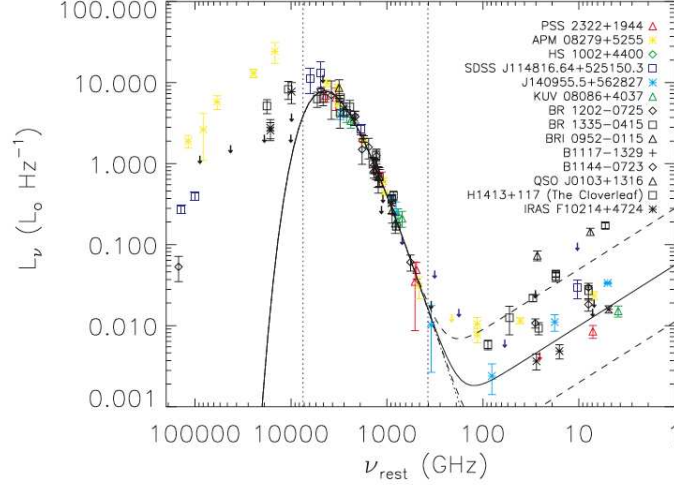


Figure 13. Composite high-redshift quasar SED (rest-frame) after normalizing the total L_{FIR} emission to the FIR luminosity of PSS 2322+1944. Figure taken from Beelen et al. (2006).

the fact that the central AGN/quasar does not contribute significantly to L_{FIR} as one would otherwise expect the quasar population to be offset from the SMG population in this plot. It is important to note however that this plot is almost certainly incomplete, in particular for high luminosities (as both FIR and CO measurements can only recover the brightest objects given the sensitivities of current instruments). Indeed, in a recent study Daddi et al. (2008) argue that BzK-selected galaxies fall off this relation significantly.

4.2. Molecular gas and PAHs in QSOs

We have already seen from Figure 15 that molecular gas is detected in a number of quasar host galaxies. Like in the case of the submillimeter galaxies, PAH emission has also been detected in some of the high-redshift quasars. A summary of all molecular gas detections is given in Solomon & Vanden Bout (2005). Some more recent CO detections of $z \sim 2$ QSOs have been presented by Coppin (2008, Figure 16) who also discuss a possible evolutionary link between QSOs and SMGs.

In a few cases, the quasars are sufficiently bright in CO that their CO emission can be imaged at high spatial resolution. Perhaps the most stunning example so far is the spatially resolved complex CO distribution of the $z=4.4$ QSO BRI1335-0417 – this source is seen when the universe was less than 2 Gyrs old. (Figure 17, Riechers et al. 2008). Its spatial and velocity structure of the molecular reservoir is inconsistent with a simple gravitationally bound disk, but resembles a merging system. The observations are consistent with a major, gas-rich (‘wet’) merger that both feeds an accreting supermassive black hole (causing the bright quasar activity), and fuels a massive starburst that builds up the stellar bulge in this galaxy. This quasar host galaxy may thus be the

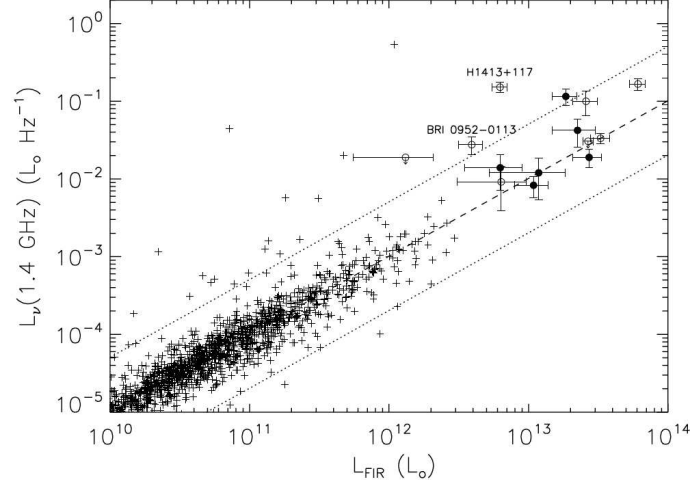


Figure 14. The radio-FIR relation for high-redshift quasars. The crosses show the IRAS 2 Jy sample of Yun et al. (2001); the circles indicate the quasars of Beelen (2003). See text for the description of the dashed/dotted lines. Figure taken from Beelen et al. (2006).

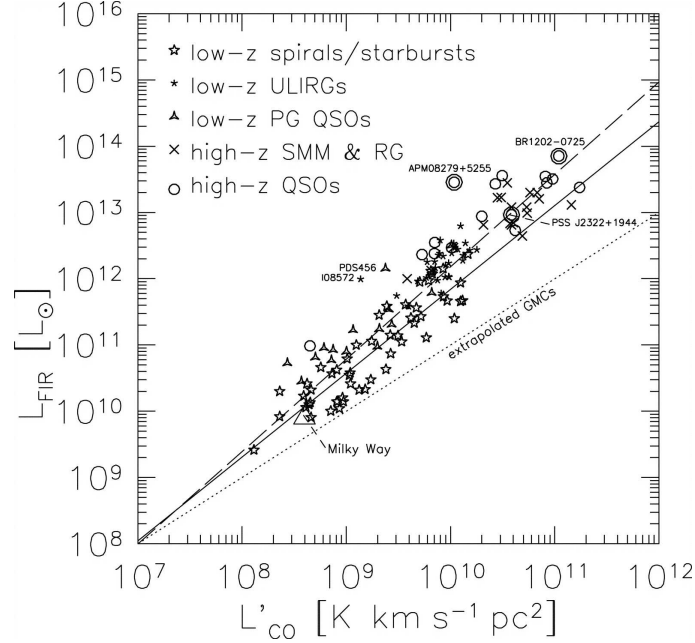


Figure 15. The star formation law: L_{FIR} (a measure for the star formation activity) as a function of L'_{CO} (a measure of the total molecular gas mass). Different galaxy classes are shown here (see text for references) – it is interesting to note that the high-redshift SMGs and QSOs cover the same parameter space, hinting at only a minor contribution to L_{FIR} by the central accreting source in the case of the QSOs. Figure taken from Riechers et al. (2006).

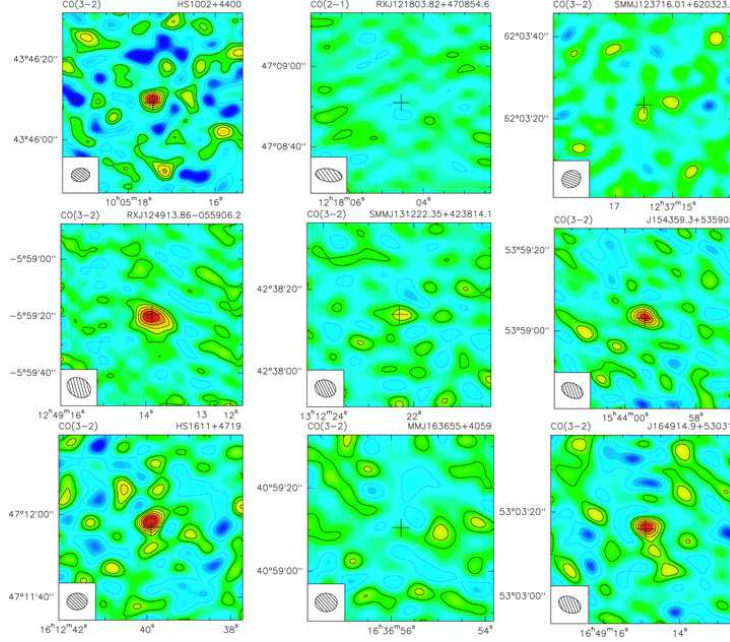


Figure 16. Detection of molecular gas in a sample of $z \sim 2$ QSOs using the Plateau de Bure interferometer. Figure taken from Coppin et al. (2008).

most direct observational evidence that $z > 4$ wet mergers at high redshift are related to AGN activity (Riechers et al. 2008).

In general, spatially and kinematically resolved observations of the molecular gas distribution offer the exciting prospect to constrain the dynamical mass of the quasar host galaxy. This mass can then be compared to the mass of the central black hole. An open question is still whether the tight relation between central black hole mass and the surrounding stellar spheroid in nearby massive ellipticals (e.g., Magorrian & Binney 1998, Gebhardt et al. 2000, Ferrarese & Merritt 2000), roughly $M_{\text{bulge}}/M_{\text{BH}} \sim 700$ is also seen at large lookback times. This would hint at a co-eval evolution of the central black hole and the surrounding stellar bulge – a remarkable scenario by the way if one considers that the black hole is nine orders of magnitudes smaller in size than the surrounding stellar bulge. As the stellar bulge can not be directly observed in quasars at high redshift (due to dimming and the very bright point source due to central accretion), obtaining an upper limit through dynamical mass measurements could be a promising way forward to constrain a possible change in this ratio. Current evidence so far points at a much lower $M_{\text{bulge}}/M_{\text{BH}}$ ratio than seen locally (e.g. Walter et al. 2004, Riechers et al. 2008b, 2009, Weiss et al. 2007, Coppin et al. 2008, Carilli & Wang 2006), though a clear answer will have to await higher sensitivity and resolution observations of a sizeable sample with ALMA.

Like in the case of the SMGs, Spitzer IRS spectroscopy also resulted in detection of PAH emission features in high-redshift quasars (Lutz et al. 2007, 2008, Martinez-Sansigre et al. 2008). As shown in the composite spectrum of $z \sim 2.5$ QSOs in Figure 18, the various PAH features are nicely detected and the PAH

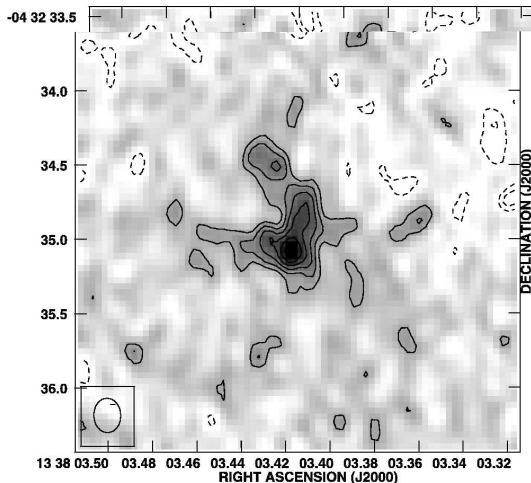


Figure 17. Spatially resolved CO distribution in the $z=4.41$ QSO BRI1335–0417 obtained with the VLA. The high resolution ($0.15''$ or ~ 1 kpc at this redshift, see beamsize in lower left corner) reveals a complex structure in the molecular gas emission, possibly hinting at a (wet) merger. Figure taken from Riechers et al. (2008).

luminosity and rest frame far-infrared luminosity correlate and extend a similar correlation seen in the case of lower luminosity local QSOs (Lutz et al. 2008). Like in the case of the SMGs, these measurement provide additional strong evidence for intense star formation activity in the hosts of these millimeter-bright QSOs. This is yet another argument that the rest-frame FIR luminosity in quasars is predominantly powered by star formation, and not AGN activity.

4.3. Prospects of dust detection in the Epoch of Reionization

As mentioned earlier, current observations are limited to the brightest objects in the early universe. ALMA, with its orders-of-magnitude increase in sensitivity, will be able to detect more typical source populations at high redshifts. It is very likely that ALMA will even reveal a major population of dusty systems at redshifts beyond 6 (when the universe was less than a Gyr old), as dust production has apparently been quite effective in the very early universe. E.g. in the case of the $z=6.42$ quasar J1148+5251, FIR emission was first detected by Bertoldi et al. (2003a). The SDSS observations, Keck spectroscopy, and HST imaging (White et al. 2003, 2005), reveal a SMBH of $2 \times 10^9 M_{\odot}$ and a very compact structure. The host galaxy has now been detected in thermal dust, non-thermal radio continuum, CO line, and [CII] $158 \mu\text{m}$ emission (Figure 19). High resolution imaging of the CO emission reveals a massive reservoir of molecular gas, $2 \times 10^{10} M_{\odot}$, distributed on a scale of 6 kpc in the host galaxy (Walter et al. 2003, 2004). The broad band SED of J1148+5251, shows a clear FIR excess, consistent with 50K dust emission and with the radio-FIR correlation for star forming galaxies (Wang et al. 2008). The high CO excitation in J1148+5251 (Bertoldi et al. 2003b, Riechers et al., *subm.*) is comparable to that seen in starburst nuclei implying dense (10^5 cm^{-3}), warm gas. The high-resolution imaging

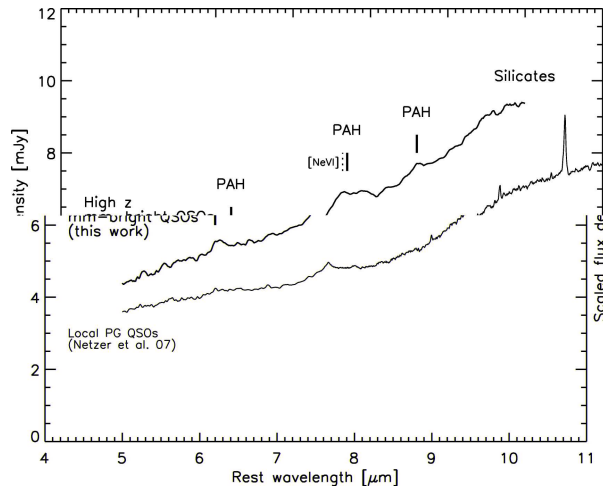


Figure 18. Spitzer IRS composite spectrum of a dozen millimeter-bright quasars at redshift $z \sim 2.5$. The PAH complexes are clearly detected, suggesting major star formation activity in these objects. Figure taken from Lutz et al. (2008).

of the [CII] emission in the host galaxy of J1148+5251 reveals an extreme starburst region with a diameter of 1.5 kpc (Maiolino et al. 2005, Walter et al. 2009), forming stars at the ‘Eddington limited’ rate of $1000 \text{ M}_{\odot} \text{ year}^{-1} \text{ kpc}^{-2}$ (Thompson et al. 2005). These measurements demonstrate that major star formation episodes are happening in the first Gyr of the Universe and that they lead to major dust production on galactic scales, as evidenced by the FIR and molecular gas measurements. Clearly, it will be critical to extend similar dust studies to less extreme systems at similar and higher redshifts. The key point to take away from this discussion is that dust production appears to be very efficient (in at least a few systems) when the Universe was less than a Gyr old (see also Maiolino 2004).

5. Concluding remarks

This review can not do justice to all the work that has been done in the field of high redshift dust emission over the last decade. But it hopefully provides an overview over the variety of strategies and techniques that have been used to characterize dust emission (and thus L_{FIR}) in systems all the way out to the epoch of reionization ($z > 6$). The field has come a long way over the last decade — however it is also clear that at the same time it is still in its infancy. The systems that are currently being studied are certainly the ‘freaks’ amongst the typical galaxy population at high redshifts, as even major local starforming systems such as Arp 220 are too faint for detection at significant redshifts ($z > 0.5$) with current facilities. The future, however, is bright: in only a couple years from now, the IRAM Plateau de Bure interferometer will have completed its upgrade to full 8 GHz bandwidth, an order of magnitude increase in bandwidth

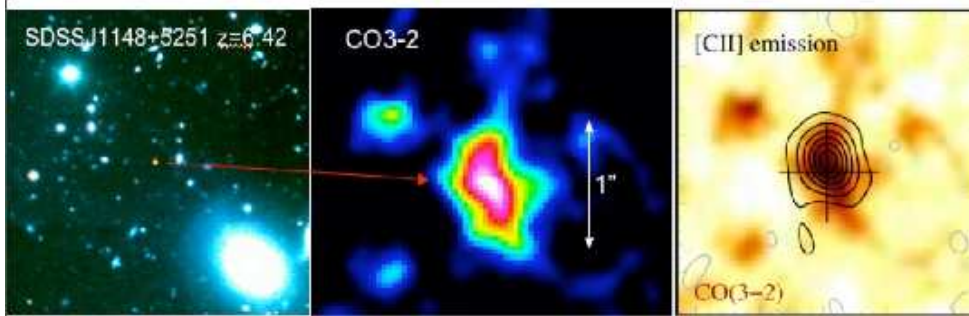


Figure 19. Images of SDSS J1148+5251 at $z = 6.42$. Left is a Keck true-color image (Djorgovski, Mahabal, and Bogosavljevic, priv. comm.). Center is the VLA image of CO 3-2 emission (Walter et al. 2004). Right is the PdBI [CII] 158 μ m image (Walter et al. 2009).

compared to Bure’s performance just a few years back. A little later, ALMA, given its site, collecting area, receiver technology and bandwidth, will afford another order of magnitude increase in sensitivity, which without doubt will revolutionize this field of research.

Acknowledgments. I thank Henrik Beuther, Chris Carilli and Rob Ivison for comments on the manuscript. It is my pleasure to thank my colleagues Frank Bertoldi, Chris Carilli, Pierre Cox, Emanuele Daddi, Helmut Dannerbauer, Thomas Greve, Dominik Riechers, Ian Smail, Ran Wang and Axel Weiss.

References

- Alloin, D., Barvainis, R., Gordon, M. A., & Antonucci, R. R. J. 1992, *A&A*, 265, 429
 Beelen, A., 2003, PhD Thesis
 Beelen, A., Cox, P., Benford, D. J., Dowell, C. D., Kovács, A., Bertoldi, F., Omont, A., & Carilli, C. L. 2006, *ApJ*, 642, 694
 Bendo, G. J., et al. 2006, *ApJ*, 645, 134
 Bertoldi, F., et al. 2000, *A&A*, 360, 92
 Bertoldi, F., Carilli, C. L., Cox, P., Fan, X., Strauss, M. A., Beelen, A., Omont, A., & Zylka, R. 2003a, *A&A*, 406, L55
 Bertoldi, F., et al. 2003b, *A&A*, 409, L47
 Bertoldi, F., et al. 2007, *ApJS*, 172, 132
 Blain, A. W., Smail, I., Ivison, R. J., Kneib, J.-P., & Frayer, D. T. 2002, *Physics Reports*, 369, 111
 Carilli, C. L., & Wang, R. 2006, *AJ*, 131, 2763
 Capak, P., et al. 2008, *ApJ*, 681, L53
 Chapman, S. C., Blain, A. W., Ivison, R. J., & Smail, I. R. 2003, *Nat*, 422, 695
 Chapman, S. C., Blain, A. W., Smail, I., & Ivison, R. J. 2005, *ApJ*, 622, 772
 Condon, J. J. 1992, *ARA&A*, 30, 575
 Condon, J. J., Cotton, W. D., & Broderick, J. J. 2002, *AJ*, 124, 675
 Coppin, K., et al. 2006, *MNRAS*, 372, 1621
 Coppin, K. E. K., et al. 2007, *ApJ*, 665, 936
 Coppin, K. E. K., et al. 2008, *MNRAS*, 389, 45
 Coppin, K., et al. 2009, arXiv:0902.4464
 Cowie, L. L., Barger, A. J., & Kneib, J.-P. 2002, *AJ*, 123, 2197

- Daddi, E., Dannerbauer, H., Elbaz, D., Dickinson, M., Morrison, G., Stern, D., & Ravindranath, S. 2008, *ApJ*, 673, L21
- Daddi, E., et al. 2009a, *ApJ*, 694, 1517
- Daddi, E., Dannerbauer, H., Krips, M., Walter, F., Dickinson, M., Elbaz, D., & Morrison, G. E. 2009b, *ApJ*, accepted, arXiv:0903.3046
- Dannerbauer, H., Lehnert, M. D., Lutz, D., Tacconi, L., Bertoldi, F., Carilli, C., Genzel, R., & Menten, K. 2002, *ApJ*, 573, 473
- Dannerbauer, H., Walter, F., & Morrison, G. 2008, *ApJ*, 673, L127
- Downes, D., et al. 1999, *A&A*, 347, 809
- Dunlop, J. 2001, *Deep Millimeter Surveys: Implications for Galaxy Formation and Evolution*, 11
- Dunlop, J. S., et al. 2004, *MNRAS*, 350, 769
- Eales, S., Bertoldi, F., Ivison, R., Carilli, C., Dunne, L., & Owen, F. 2003, *MNRAS*, 344, 169
- Evans, A. S., Frayer, D. T., Surace, J. A., & Sanders, D. B. 2001, *AJ*, 121, 1893
- Ferrarese, L., & Merritt, D. 2000, *ApJ*, 539, L9
- Fixsen, D. J., Bennett, C. L., & Mather, J. C. 1999, *ApJ*, 526, 207
- Gao, Y., & Solomon, P. M. 2004, *ApJS*, 152, 63
- Gawiser, E., et al. 2006, *ApJS*, 162, 1
- Gebhardt, K., et al. 2000, *ApJ*, 539, L13
- Genzel, R., Baker, A. J., Tacconi, L. J., Lutz, D., Cox, P., Guilloteau, S., & Omont, A. 2003, *ApJ*, 584, 633
- Greve, T. R., et al. 2005, *MNRAS*, 359, 1165
- Greve, T. R., Pope, A., Scott, D., Ivison, R. J., Borys, C., Conselice, C. J., & Bertoldi, F. 2008, *MNRAS*, 389, 1489
- Greve, T. R., Weiss, A., Walter, F., Smail, I., et al., 2009, *ApJ*, *subm.*
- Guelin, M., Zylka, R., Mezger, P. G., Haslam, C. G. T., & Kreysa, E. 1995, *A&A*, 298, L29
- Hughes, D. H., et al. 1998, *Nat*, 394, 241
- Ivison, R. 2001, *Cosmological Physics with Gravitational Lensing*, 233
- Ivison, R. J., et al. 2002, *MNRAS*, 337, 1
- Ivison, R. J., et al. 2005, *MNRAS*, 364, 1025
- Ivison, R. J., et al. 2007, *MNRAS*, 380, 199
- Knudsen, K. K., van der Werf, P. P., & Kneib, J.-P. 2008, *MNRAS*, 384, 1611
- Knudsen, K. K., et al. 2006, *MNRAS*, 368, 487
- Lutz, D., Valiante, E., Sturm, E., Genzel, R., Tacconi, L. J., Lehnert, M. D., Sternberg, A., & Baker, A. J. 2005, *ApJ*, 625, L83
- Lutz, D., et al. 2007, *ApJ*, 661, L25
- Lutz, D., et al. 2008, *ApJ*, 684, 853
- Maiolino, R., Schneider, R., Oliva, E., Bianchi, S., Ferrara, A., Mannucci, F., Pedani, M., & Roca Sogorb, M. 2004, *Nat*, 431, 533
- Maiolino, R., et al. 2005, *A&A*, 440, L51
- Magorrian, J., et al. 1998, *AJ*, 115, 2285
- Martínez-Sansigre, A., Lacy, M., Sajina, A., & Rawlings, S. 2008, *ApJ*, 674, 676
- Meijerink, R., Tilanus, R. P. J., Dullemond, C. P., Israel, F. P., & van der Werf, P. P. 2005, *A&A*, 430, 427
- Menéndez-Delmestre, K., et al. 2007, *ApJ*, 655, L65
- Mooney, T. J., & Solomon, P. M. 1988, *ApJ*, 334, L51
- Mortier, A. M. J., et al. 2005, *MNRAS*, 363, 563
- Neri, R., et al. 2003, *ApJ*, 597, L113
- Omont, A., Beelen, A., Bertoldi, F., Cox, P., Carilli, C. L., Priddey, R. S., McMahon, R. G., & Isaak, K. G. 2003, *A&A*, 398, 857
- Perera, T. A., et al. 2008, *MNRAS*, 391, 1227
- Pope, A., et al. 2008, *ApJ*, 675, 1171
- Riechers, D. A., et al. 2006, *ApJ*, 650, 604

- Riechers, D. A., Walter, F., Carilli, C. L., Bertoldi, F., & Momjian, E. 2008, *ApJ*, 686, L9
- Riechers, D. A., Walter, F., Brewer, B. J., Carilli, C. L., Lewis, G. F., Bertoldi, F., & Cox, P. 2008b, *ApJ*, 686, 851
- Riechers, D. A., Walter, F., Carilli, C. L., & Lewis, G. F. 2009, *ApJ*, 690, 463
- Schinnerer, E., et al. 2008, *ApJ*, 689, L5
- Scott, K. S., et al. 2008, *MNRAS*, 385, 2225
- Scoville, N. Z., Frayer, D. T., Schinnerer, E., & Christopher, M. 2003, *ApJ*, 585, L105
- Scoville, N., et al. 2007, *ApJS*, 172, 1
- Smail, I., Ivison, R. J., & Blain, A. W. 1997, *ApJ*, 490, L5
- Smail, I. 2002, *Ap&SS*, 281, 453
- Smail, I., Ivison, R. J., Blain, A. W., & Kneib, J.-P. 2002, *MNRAS*, 331, 495
- Smail, I., Ledlow, M. J., Owen, F. N., Keel, W. C. I. R. J., & Morrison, G. E. 2003, *Revista Mexicana de Astronomia y Astrofisica Conference Series*, 17, 214
- Smail, I. 2006, Review for 2005 SSC Conference "Infrared Diagnostics of Galaxy Evolution", *astro-ph/0603635*
- Solomon, P. M., Downes, D., Radford, S. J. E., & Barrett, J. W. 1997, *ApJ*, 478, 144
- Solomon, P. M., & Vanden Bout, P. A. 2005, *ARA&A*, 43, 677
- Tacconi, L. J., et al. 2006, *ApJ*, 640, 228
- Tacconi, L. J., et al. 2008, *ApJ*, 680, 246
- Thomas, H. C., Dunne, L., Clemens, M. S., Alexander, P., Eales, S., & Green, D. A. 2002, *MNRAS*, 329, 747
- Thompson, T. A., Quataert, E., & Murray, N. 2005, *ApJ*, 630, 167
- Valiante, E., Lutz, D., Sturm, E., Genzel, R., Tacconi, L. J., Lehnert, M. D., & Baker, A. J. 2007, *ApJ*, 660, 1060
- Voss, H., 2003, Diploma Thesis, Bonn University
- Walter, F., et al. 2003, *Nat*, 424, 406
- Walter, F., Carilli, C., Bertoldi, F., Menten, K., Cox, P., Lo, K. Y., Fan, X., & Strauss, M. A. 2004, *ApJ*, 615, L17
- Walter, F., Riechers, D., Cox, P., Neri, R., Carilli, C., Bertoldi, F., Weiss, A., & Maiolino, R. 2009, *Nat*, 457, 699
- Wang, R., et al. 2007, *AJ*, 134, 617
- Wang, R., et al. 2008, *ApJ*, 687, 848
- Weiß, A., Downes, D., Neri, R., Walter, F., Henkel, C., Wilner, D. J., Wagg, J., & Wiklind, T. 2007, *A&A*, 467, 955
- Weiß, A., Kovács, A., Güsten, R., Menten, K. M., Schuller, F., Siringo, G., & Kreysa, E. 2008, *A&A*, 490, 77
- White, R. L., Becker, R. H., Fan, X., & Strauss, M. A. 2003, *AJ*, 126, 1
- White, R. L., Becker, R. H., Fan, X., & Strauss, M. A. 2005, *AJ*, 129, 2102
- Younger, J. D., et al. 2007, *ApJ*, 671, 1531
- Yun, M. S., Reddy, N. A., & Condon, J. J. 2001, *ApJ*, 554, 803